Inorg. Chem. **2007**, *46*, 6950–6957

Single-Boron Complexes of N-Confused and N-Fused Porphyrins

Anna Młodzianowska, Lechosław Latos-Grażyński,* Ludmiła Szterenberg, and Marcin Stępień

Department of Chemistry, University of Wrocław, 14 F. Joliot-Curie Street, Wrocław 50 383, Poland

Received April 4, 2007

Boron(III) has been inserted into N-confused porphyrin, (*N*CP*H*)H_2 (**1**), and N-fused porphyrin, (*N*FP)H (**2**). The reaction of dichlorophenylborane and **1** yields σ-phenylboron N-confused porphyrin (**4**). The boron atom is bound by two pyrrolic nitrogen atoms and the σ-phenyl ligand. The N-confused pyrrole ring is not involved in the direct coordination because the C(21)–H fragment remains intact. A reaction between $PhBCl_2$ and N-fused porphyrin produces σ-phenylboron N-fused porphyrin ($\mathbf{3}^+$). **4** converts quantitatively into $\mathbf{3}^+$ under protonation. In σ-phenylboron *N*-fused porphyrin [(*N*FP)BPh]Cl, the coordinating environment of boron(III) resembles a distorted trigonal pyramid, with the nitrogen atoms occupying equatorial positions and with the phenyl ligand lying at the unique apex. Boron(III) is displaced by 0.547(4) Å from the N_3 plane. The B–N distances are as follows: B–N(22), 1.559(4) Å; B–N(23), 1.552(4) Å; B–N(24), 1.568(4) Å; B–C_{ipsoPh}, 1.621(4) Å. $\mathbf{3}^+$ can be classified as a boronium cation considering a filled octet and a complete coordination sphere. $\mathbf{3}^+$ is susceptible to alkoxylation at the inner C(9) carbon atom, yielding **5**-OR. The addition of acid results in protonation of the alkoxy group and elimination of alcohol, restoring the original $\mathbf{3}^+$. Density functional theory has been applied to model the molecular and electronic structure of **4**, $\mathbf{3}^+$, and syn and anti isomers of methoxy adducts **5**-OMe.

Introduction

The insertion of boron(III) into porphyrins yields remarkable structures with two boron atoms in the core of macrocycle, clearly revealing a mismatch between the boron ionic radius and the porphyrin core.[1−6] Typically, only two nitrogen atoms of the porphyrin coordinate to the single boron ion. In the case of an extended porphyrin, two coordinated boron ions are separated well enough[6] so that the coordination pattern resembles that well-characterized for BF_2-coordinated dipyrromethene complexes.[7−10] Coordination of a single boron ion in porphyrin-like surroundings was solely observed for subphthalocyanines,[11,12] subporphyrazine,[13] tribenzosubporphyrine,[14] and subporphine,[15] contracted homologues of phthalocyanines and porphyrins where introduction of the boron atom warranted a template synthesis.[14−16] Recently, the very first insertion of a single boron atom into subpyriporphyrin, a [14]triphyrin(1.1.1) homologue with an embedded pyridine moiety, has been reported.[17]

Chart 1

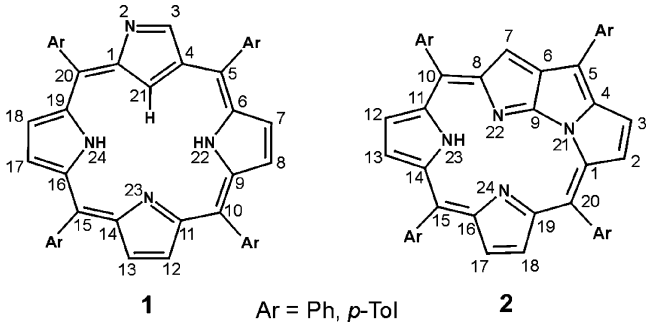

1 **2**

This contribution presents a new type of single boron porphyrinoids. Namely, the boron has been inserted into appropriately prearranged macrocycles: N-confused porphyrin **1**,[18,19] and N-fused porphyrin **2** (Chart 1).[20,21] Orig-

* To whom correspondence should be addressed. E-mail: llg@wchuwr.chem.uni.wroc.pl.

(1) Belcher, W. J.; Boyd, P. D. W.; Brothers, P. J.; Liddell, M. J.; Rickard, C. E. F. *J. Am. Chem. Soc.* **1994**, *116*, 8416−8417.
(2) Belcher, W. J.; Breede, M.; Brothers, P. J.; Rickard, C. E. F. *Angew. Chem., Int. Ed.* **1998**, *37*, 1112−1114.
(3) Senge, M. O. *Angew. Chem., Int. Ed.* **1998**, *37*, 1071−1072.
(4) Weiss, A.; Pritzkow, H.; Brothers, P. J.; Siebert, W. *Angew. Chem., Int. Ed.* **2001**, *40*, 4182−4184.
(5) Brothers, P. J. *J. Porphyrins Phthalocyanines* **2002**, *6*, 259−267.
(6) Köhler, T.; Hodgson, M. C.; Seidel, D.; Veauthier, J. M.; Meyer, S.; Lynch, V.; Boyd, P. D. W.; Brothers, P. J.; Sessler, J. L. *Chem. Commun.* **2004**, 1060−1061.
(7) Shen, Z.; Röhr, H.; Rurack, K.; Uno, H.; Spieles, M.; Schulz, B.; Reck, G.; Ono, N. *Chem.—Eur. J.* **2004**, *10*, 4853−4871.
(8) Burghart, A.; Kim, H. J.; Welch, M. B.; Thoresen, L. H.; Reibenspies, J.; Burgess, K.; Bergström, F.; Johansson, L. B. A. *J. Org. Chem.* **1999**, *64*, 7813−7819.
(9) Kim, H.; Burghart, A.; Welch, M. B.; Reibenspies, J.; Burgess, K. *Chem. Commun.* **1999**, 1889−1890.
(10) Ziessel, R.; Goze, C.; Ulrich, G.; Césario, M.; Retailleau, P.; Harriman, A.; Rostron, J. P. *Chem.—Eur. J.* **2005**, *11*, 7366−7378.
(11) Meller, A.; Ossko, A. *Monatsh. Chem.* **1972**, *103*, 150.
(12) Claessens, C. G.; Gonzáles-Rodríguez, D.; Torres, T. *Chem. Rev.* **2002**, *102*, 835−853.
(13) Rauschnabel, J.; Hanack, M. *Tetrahedron Lett.* **1995**, *36*, 1629−1632.
(14) Inokuma, Y.; Kwon, J. H.; Ahn, T. K.; Yoo, M.-C.; Kim, D.; Osuka, A. *Angew. Chem., Int. Ed.* **2006**, *45*, 961−964.
(15) Kobayashi, N.; Takeuchi, Y.; Matsuda, A. *Angew. Chem., Int. Ed.* **2007**, *46*, 758−760.

10.1021/ic700647v CCC: $37.00
Published on Web 07/17/2007

Scheme 1. Synthesis of "Single"-Boron Complexes 3^+ and **4**

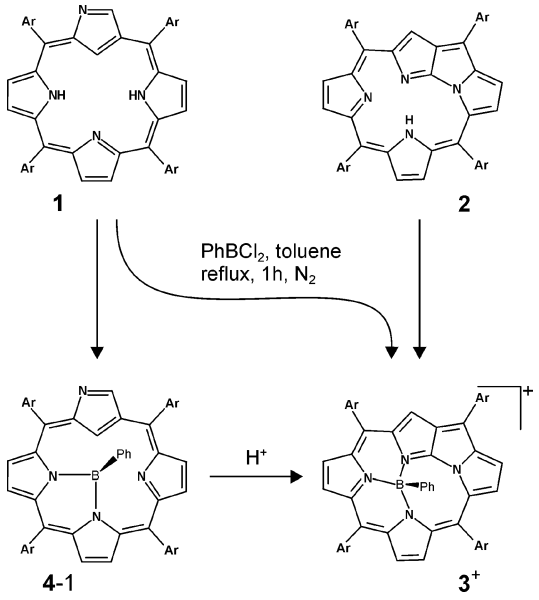

inally, N-fused porphyrin **2** was chosen as a suitable environment for the boron entrapment considering the contracted size of the three-nitrogen core. Up to the present, Furuta and co-workers have demonstrated that N-fused porphyrin coordinates selected metal ions in a specific sitting-a-top manner with obvious preference for the very high oxidation state and consistently relatively small ionic radii of metal ions.[22] We presume that N-confused porphyrin provides an appropriate macrocyclic setting for coordination of main group metal ions and metalloids known for their small ionic radii, exemplified here by boron(III).[23]

Results and Discussion

***σ*-Phenylboron N-Fused Porphyrins.** The synthetic work of this study has been summarized in Scheme 1.

N-Fused porphyrin **2** reacts with $PhBCl_2$ in toluene, yielding *σ*-phenylboron(III) N-fused porphyrin, $[(NFP)BPh]^+$ ($\mathbf{3}^+$), wherein the macrocycle acts as a monoanionic tridentate ligand. After the boron(III) insertion, compound $\mathbf{3}^+$ is isolated as the chloride or tetrafluoroborate salt, as described in the Experimental Section. The electronic spectrum of $\mathbf{3}^+$ is similar to that of **2** (Figure 1).

The molecular structure of $\mathbf{3}^+$ has been determined in X-ray diffraction (Figure 2). The coordinating environment of boron(III) resembles a distorted trigonal pyramid, with the nitrogen atoms occupying equatorial positions and with

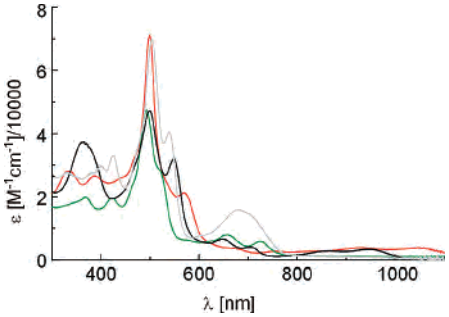

Figure 1. UV−vis spectra of **2** (black line), $\mathbf{3}^+$ (red line), **4** (green line), and **5**-OMe (gray line) in dichloromethane.

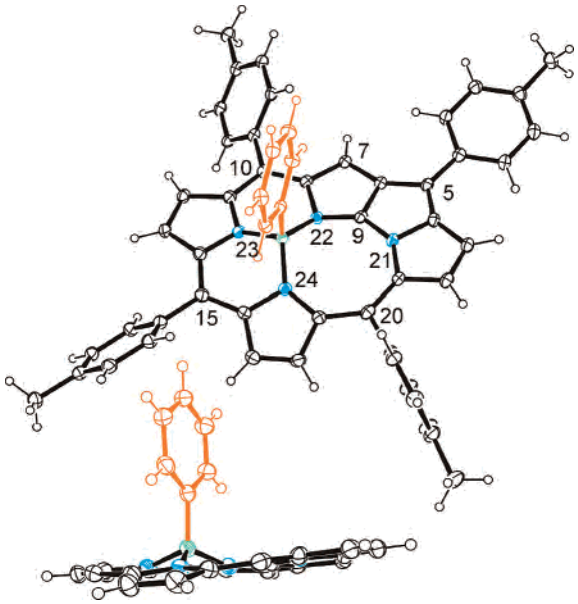

Figure 2. Molecular structure of $[\mathbf{3}^+]$-Cl (top, perspective view; bottom, side view with phenyl groups omitted for clarity). The thermal ellipsoids represent 30% probability. Disordered solvent molecules and the chloride anion are removed for clarity.

the phenyl ligand lying at the unique apex. Boron(III) is displaced by 0.547(4) Å from the N_3 plane (Figure 2). The B−N distances are as follows: B−N(22), 1.559(4) Å; B−N(23), 1.552(4) Å; B−N(24), 1.568(4) Å. All B−N(pyrrolic) bond lengths are comparable to the B−N distances in boron porphyrins[1,2,4,6] but slightly longer than those for boron subphthalocyanines[12,13,24,25] or boron tribenzosubporphyrines.[14] The B−C bond length approaches that determined for *σ*-phenylboron subphthalocyanine, 1.597 Å.[13]

Three of the *meso*-*p*-tolyl substituents, namely, those attached to carbons 10, 15, and 20, form sharp dihedral angles with the macrocyclic plane (ranging from 46 to 80°). This conformational feature is typical of meso-substituted porphyrins. In contrast, the 5-*p*-tolyl substituent is almost coplanar with the macrocycle, forming a dihedral angle of 7.5°. This difference results from the reduction of steric repulsion between the macrocycle and the tolyl ring, caused by ring fusion. Specifically, the C(4)−C(5)−C(6) angle, contained in a five-membered ring, is only 104.5(3)°, much less than the respective angles at other meso positions (119−134°). Consequently, hydrogens H(7) and H(3) are moved away from the 5-tolyl ring, thereby enabling a coplanar orientation of the substituent. Such a structural pattern, as

(16) Torres, T. *Angew. Chem., Int. Ed.* **2006**, *45*, 2834−2837.
(17) Myśliborski, R.; Latos-Grażyński, L.; Szterenberg, L.; Lis, T. *Angew. Chem., Int. Ed.* **2006**, *45*, 3670−3674.
(18) Chmielewski, P. J.; Latos-Grażyński, L.; Rachlewicz, K.; Głowiak, T. *Angew. Chem., Int. Ed. Engl.* **1994**, *33*, 779−781.
(19) Furuta, H.; Asano, T.; Ogawa, T. *J. Am. Chem. Soc.* **1994**, *116*, 767−768.
(20) Furuta, H.; Ishizuka, T.; Osuka, A.; Ogawa, T. *J. Am. Chem. Soc.* **2000**, *122*, 5748−5757.
(21) Furuta, H.; Ishizuka, T.; Osuka, A.; Ogawa, T. *J. Am. Chem. Soc.* **1999**, *121*, 2945−2946.
(22) Toganoh, M.; Ishizuka, T.; Furuta, H. *Chem. Commun.* **2004**, 2464−2465.
(23) Toganoh, M.; Ikeda, S.; Furuta, H. *Chem. Commun.* **2005**, 4589−4591.

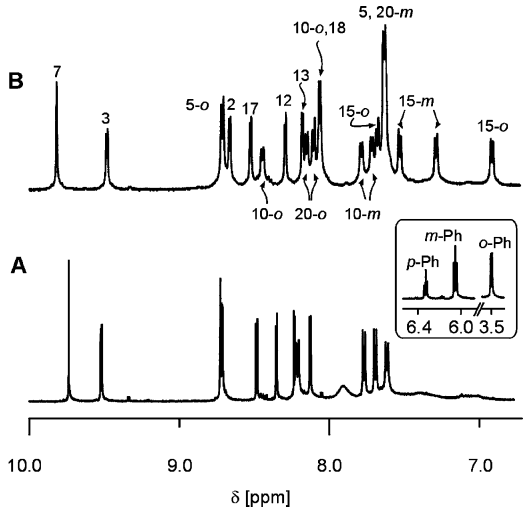

Figure 3. ^{1}H NMR spectra: (A) $\mathbf{3}^+$, dichloromethane-d_2, 298 K; (B) $\mathbf{3}^+$, dichloromethane-d_2, 198 K. The inset in trace A shows the σ-phenyl resonances. Peak labels follow a systematic position numbering of the macrocycle or denote proton groups: o, m, and p are ortho, meta, and para positions of *meso*-*p*-tolyl rings, respectively.

seen here for $\mathbf{3}^+$, was previously noted for the free-base N-fused porphyrin.[20] Actually, the ^{1}H NMR studies carried out for $\mathbf{3}^+$ demonstrate clearly the influence of this structural factor on the dynamic rearrangement involving the *p*-tolyl ring rotation.

Cyclic voltammetry demonstrates that $\mathbf{3}^+$ undergoes two consecutive, reversible, one-electron reductions with half-wave potentials of (1) −602 mV and (2) −1196 mV, yielding $\mathbf{3}^\bullet$ (σ-phenylboron N-fused porphyrin radical, [(*N*FP)BPh]$^\bullet$) and subsequently the monoanion $\mathbf{3}^-$ (potentials vs Fc/Fc$^+$, CH_2Cl_2, TBAP). Thus, the reduction potentials of $\mathbf{3}^+$ have been anodically shifted with respect to the free-base N-fused porphyrin (the first oxidation potential at 80 mV and the first reduction potential at −1370 mV vs Fc/Fc$^+$, CH_2Cl_2, $TBABF_4$).[20,22] The solution of **[3$^+$]**-Cl, which typically contains an admixture of $\mathbf{3}^\bullet$ (toluene, 298 K) exhibits a single line at $g = 2.0027$ in the electron paramagnetic resonance (EPR) spectrum, which is consistent with the anion radical electronic structure.

Because of the boron(III) coordination, the pyrrole ^{1}H NMR resonances of $\mathbf{3}^+$ are slightly shifted with respect to **2**. The most notable feature is the marked upfield positions of the axially coordinated σ-phenyl (*o*-H, 3.50 ppm; *m*-H, 6.05 ppm; *p*-H, 6.33 ppm), although less pronounced than those for regular σ-phenyl diamagnetic metalloporphyrins[26] but similar to those for previously reported σ-phenylboron subphthalocyanine (SubPh)BPh[13] and σ-phenylboron subpyriporphyrin.[17] These observations readily confirm the aromatic character of $\mathbf{3}^+$, allowing the 18e π-delocalization path.[21] Well-resolved ^{1}H NMR spectra of $\mathbf{3}^+$ can be obtained under carefully controlled conditions (Figure 3). In each case, the presence of even a minute amount of the radical $\mathbf{3}^\bullet$ leads to significant line broadening and shortening of T_1 relaxation times, confirming fast electron exchange between differently oxidized forms of **3**.[27,28] Typically, the addition of $AgBF_4$, which acted as the oxidizing reagent, was sufficient to remove the residual $\mathbf{3}^\bullet$.

The complete assignment of all ^{1}H NMR resonances for $\mathbf{3}^+$, as shown in Figure 3, has been obtained by 2D ^{1}H NMR COSY and NOESY experiments using the unique nuclear Overhauser effect (NOE) correlation between H(7) and *o*-H(5-*p*-tolyl) as a starting point. The peculiar downfield positions of H(7) and H(3) resonances due to the ring current effect of the common adjacent *meso*-*p*-tolyl ring afforded the initial assignment of these particular resonances. Actually, this initial assignment is consistent with the ^{1}H NMR spectroscopic pattern of the selectively brominated 7-bromo N-fused and 7,12,13-tribromo N-fused porphyrins.[20] The steric hindrance of the C(7)−H and C(12)−H fragments is smaller than that created by any other two β-CH fragments flanking *p*-tolyls as discussed above. This structural factor lowers the rotation barrier in comparison to other meso positions, which results in the fast rotation of this substituent in the whole investigated 178−353 K temperature range for the series of solvents (chloroform-*d*, dichloromethane-d_2, acetonitrile-d_3, and methanol-d_4), presenting consistently an AA′BB′ spectroscopic pattern. On the contrary, as the temperature was gradually lowered, all other *p*-tolyl resonances broaden and eventually split into two signals, reflecting the asymmetry with respect to the porphyrin plane (Figure 3, trace B).

σ-Phenylboron N-Confused Porphyrin. The reaction of dichlorophenylborane and **1** results in a direct insertion, yielding σ-phenylboron N-confused porphyrin [(*N*CP*H*)BPh, **4**; Scheme 1]. Initially, apart from **4** a small amount of $\mathbf{3}^+$ has been detected in the reaction products. A remarkable quantitative conversion of **4** into $\mathbf{3}^+$ requires the addition of an acid. **4** is aromatic, as is readily demonstrated by upfield-shifted resonances of axial σ-phenyl (*o*-H, 3.37 ppm; *m*-H, 5.88 ppm; *p*-H, 6.00 ppm; Figure 4).

In **4**, the boron atom is bound by two equatorially coordinated nitrogen atoms having the σ-phenyl ligand in the third position. The coordination of a single boron ion to two pyrrolic nitrogen atoms seems to be typical for boron porphyrins.[1−6] Actually, such a coordination mode has been suggested by the density functional theory (DFT) optimization carried out for **4**-1 and **4**-2 [N(23)−N(24) vs N(22)−N(23) coordination modes for **4**-1 and **4**-2, respectively] as discussed below. Scheme 1 presents only one from two possible isomers **4**-1, intuitively preferred because of an obvious prearrangement required for the N-confused−N-fused porphyrin transformation. The N-confused pyrrole is not involved in the strong coordination because the C−H fragment remains intact and has been detected in the ^{1}H NMR spectrum at −2.23 ppm (Figure 4). Still, the interaction of the boron ion and C(21)−H is reflected by carbon chemical shifts. The C(21) resonance of **4** has been detected at 73.4 ppm as compared to the chemical shift of **1**

(24) Fukuda, T.; Olmstead, M. M.; Durfee, W. S.; Kobayashi, N. *Chem. Commun.* **2003**, 1256−1257.
(25) Potz, R.; Göldner, M.; Hückstädt, H.; Cornelissen, U.; Tulass, A.; Homborg, H. *Z. Anorg. Allg. Chem.* **2000**, *626*, 588−596.
(26) Guilard, R.; Zrineh, A.; Tabard, A.; Endo, A.; Han, B. C.; Lecomte, C.; Souhassou, M.; Habbou, A.; Ferhart, M.; Kadish, K. M. *Inorg. Chem.* **1990**, *29*, 4476−4482.
(27) Sprutta, N.; Świderska, M.; Latos-Grażyński, L. *J. Am. Chem. Soc.* **2005**, *127*, 13108−1309.
(28) Nervi, C.; Gobetto, R.; Milone, L.; Viale, A.; Rosenberg, E.; Rokhsana, D.; Fiedler, J. *Chem.—Eur. J.* **2003**, *9*, 5479.

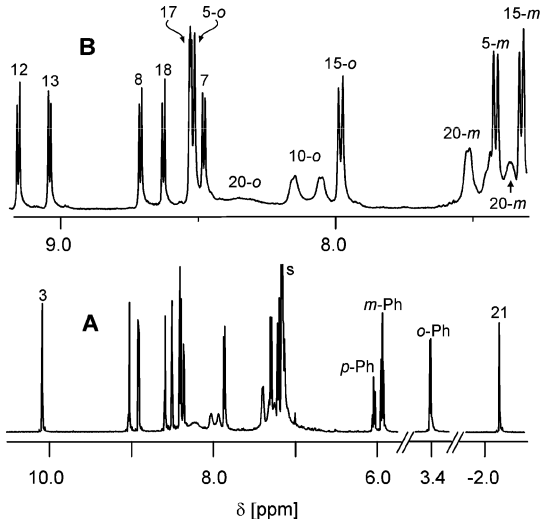

Figure 4. ^{1}H NMR spectra of **4**: (A) whole spectroscopic range (benzene-d_6, 298 K); (B) detailed assignment of pyrrole resonances. Peak labels follow a systematic position numbering of the macrocycle or denote proton groups: o, m, and p are ortho, meta, and para positions of *meso*-*p*-tolyl rings, respectively.

Chart 2. **5**-OR

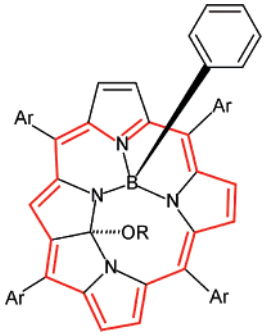

(99.6 ppm). The analogous remarkable upfield shifts relative to the free base have been previously reported for diamagnetic complexes of carbaporphyrinoids, where the side-on interaction between the metal ion and the C−H fragment has been confirmed.[29−32]

Reactions with Alkoxides. Formally, $\mathbf{3}^+$ could be treated as a tetracoordinate boron cation classified as a boronium cation. Such cations have been extensively explored, certainly demonstrating their relative stability, which results from a filled octet and a complete coordination sphere.[33] While four-coordinate cations are well-known, there are very few supported by a tridentate macrocyclic ligand.[17]

Of particular importance is the observation that $\mathbf{3}^+$ is susceptible to alkoxylation at the C(9) carbon center. Thus, $\mathbf{3}^+$ immediately reacts with methoxide dissolved in the methanol to yield a novel complex, **5**-OMe (Chart 2). Judging by the ^{1}H NMR spectrum of the reaction mixture, the process

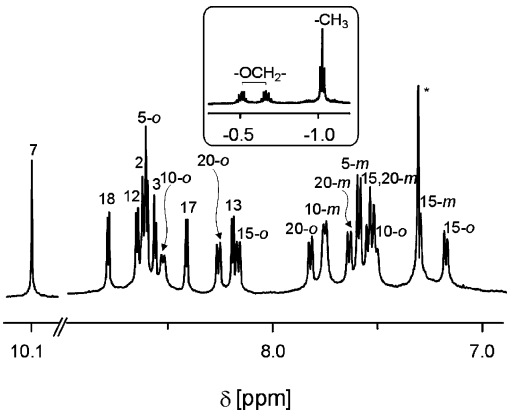

Figure 5. ^{1}H NMR spectrum of **5**-OMe (dichloromethane-d_2, 203 K). The inset presents the ethoxide resonances of **5**-OEt.

is nearly quantitative. The electronic absorption spectrum of **5**-OMe bears some resemblance to the maternal $\mathbf{3}^+$ compound (Figure 1). The ^{1}H NMR spectrum of **5**-OMe indicates the presence of a stronger aromatic ring current than that of $\mathbf{3}^+$, as reflected by upfield relocation of the phenyl resonances (*o*-H, 1.88 ppm; *m*-H, 5.25 ppm; *p*-H, 5.63 ppm). The −OMe group gives a singlet at −0.52 ppm ($CDCl_3$), which shows dipolar couplings to H(5-ortho), H(15-ortho), and H(7) in the NOESY map. This upfield shift is diagnostic for alkoxyl groups located in the center of aromatic macrocycles, as is found, for instance, with the methoxy group of dimethoxo(*meso*-tetraphenylporphyrinato)-germanium(IV), −2.57 ppm,[34] or the ethoxy ligand of diethoxo(*meso*-tetraphenylporphyrinato)germanium(IV)): methylene, −2.27(q) ppm, and methyl, −1.94(t) ppm.[35] Subsequently, the upfield-located resonances have been detected for analogous ethoxy and *n*-butoxy complexes, **5**-OEt and **5**-OBu. The diagnostic set of two complex multiplets at −0.52 and −0.68 ppm has been assigned to the ethoxy methylene group (Figure 5, inset). The strong difference of the chemical shifts detected for the two methylene multiplets, accompanied by the methyl triplet at −1.04 ppm, is due to the diastereotopic effect because the chirality center is located on the tetrahedral hybridized C(9) carbon atom. The pronounced diasterotopic effect has been readily detected for methylene groups of **5**-OBu, yielding six one-hydrogen resonances: −0.42, −0.61, −0.74, −0.85, −0.91, and −0.99 ppm. The addition of sodium 2-hydroxyethoxide to **[3**$^+$**]**-Cl yields the monomeric (2-hydroxyethoxy) derivative **5**-O$(CH_2)_2$-OH (2-hydroxyethoxy resonances at +1.50, −0.01, −0.74, and −1.00 ppm). The analogous experiment with sodium 4-hydroxybutoxide yielded monomeric **5**-O$(CH_2)_4$OH with a spectroscopic pattern resembling that of **5**-OBu. The addition of TFA to **5**-OR results in protonation of the alkoxy group and elimination of alcohol, restoring $\mathbf{3}^+$. The appropriate examples of inner macrocyclic attack were documented in the literature.[36]

(29) Stępień, M.; Latos-Grażyński, L. *Chem.—Eur. J.* **2001**, *7*, 5113−5117.
(30) Stępień, M.; Latos-Grażyński, L.; Szterenberg, L.; Panek, J.; Latajka, Z. *J. Am. Chem. Soc.* **2004**, *126*, 4566−4580.
(31) Chmielewski, M. J.; Pawlicki, M.; Sprutta, N.; Szterenberg, L.; Latos-Grażyński, L. *Inorg. Chem.* **2006**, *45*, 8664−8671.
(32) Pawlicki, M.; Latos-Grażyński, L.; Szterenberg, L. *Inorg. Chem.* **2005**, *44*, 9779−9786.
(33) Piers, W. E.; Bourke, S. C.; Conroy, K. D. *Angew. Chem., Int. Ed.* **2005**, *44*, 5016−5036.
(34) Lin, S.-J.; Chen, Y.-J.; Chen, J.-H.; Liao, F.-L.; Wang, S.-L.; Wang, S.-S. *Polyhedron* **1997**, *16*, 2842−2850.
(35) Balch, A. L.; Cornman, C. R.; Olmstead, M. M. *J. Am. Chem. Soc.* **1990**, *112*, 2963−2969.
(36) Fukuda, T.; Ogi, Y.; Kobayashi, N. *Chem. Commun.* **2006**, 159−161.

Two other routes for the formation of **5**-OR have also been considered. One of them involves the use of a fifth coordination site, producing the hypervalent boron complexes that contain five regular boron−ligand bonds.[37−40] Alternatively, the coordination can occur through dissociation of the equatorial B−N bond to provide an open coordination site for the incoming alkoxide. The analogous mechanism was considered in the mechanism of propylene oxide polymerization catalyzed by chelated borates of the general formula LB(OR) (where L is a tridentate ($-O_2N$) ligand and R = Me, Et, *n*-Pr, and *n*-Bu).[41]

Actually, to release internal molecular strains of $\mathbf{3}^+$, the new aromatic carbaporphyrinoid (R = Me, Et, *n*-Bu, and 2-hydroxyethoxide), stabilized by *σ*-phenylboron coordination (**5**-OR), has been formed (Chart 2). A new macrocyclic frame bears one alkoxy substituent attached to C(9) of the initially N-fused porphyrin. The modified macrocycle acts as dianionic ligand and preserves the 18e *π*-delocalization pathway. Significantly, the ^{13}C NMR chemical shift of the diagnostic C(9) resonance of **5**-OEt is 94.8 ppm upfield with respect to $\mathbf{[3}^+\mathbf{]}$-BF_4. The assignment of this resonance has been unambiguously determined by an heteronuclear multiple-bond correlation experiment, where correlation between C(9) and the α-methylene hydrogen atoms of the ethoxy group has been detected. The ^{13}C NMR chemical shift of C(9) is consistent with the tetrahedral hybridization considering its substitution by three electronegative atoms. The effect of such substitutions on the ^{13}C NMR chemical shift was previously documented for pyrrole-appended derivatives of O-confused oxaporphyrin.[42]

The reversible trigonal−tetrahedral exchange process at the C(9) carbon atom causes significant structural changes in the molecular structure. In principle, this process may create two geometrical isomers affording the syn and anti location of the alkoxy group with respect to the *σ*-phenyl ligand, although only the anti form was observed, as confirmed by NOESY experiments. The peculiar regioselectivity results from the steric hindrance imposed by the *σ*-phenyl ligand, which excludes one side of the porphyrin from an attack by a nucleophile.

DFT Calculations. To address the issues of the relative stabilities of isomers considered for **4** (**4**-1 and **4**-2) and **5** (**5**-anti and **5**-syn) species, we have carried out DFT calculations by performing full geometry optimizations at the B3LYP/6-31G** level. Initially, analogous DFT calculations have been carried out for $\mathbf{3}^+$ using the geometry determined by X-ray crystallography as a starting point of the optimization procedure (Figure 6).

The optimized structural parameters are contained in the Supporting Information. The optimized bond lengths of $\mathbf{3}^+$ resemble those found by X-ray crystallography. The differences of the bond lengths between the DFT-optimized and crystal values are in the range of a few hundredths of angstroms.

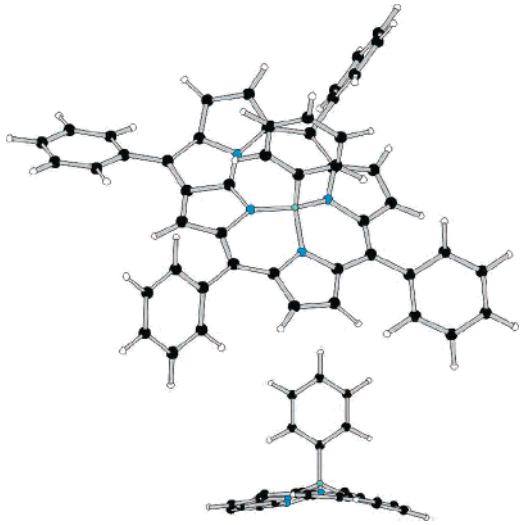

Figure 6. DFT-optimized structure of $\mathbf{3}^+$ (top, perspective view; bottom, side view).

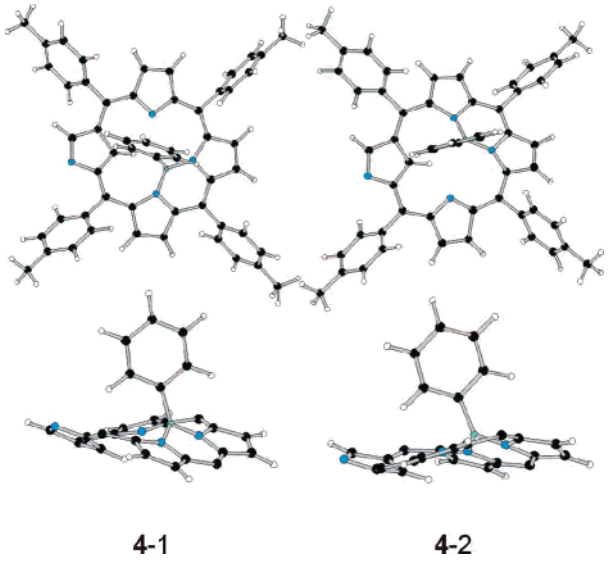

4-1 **4-2**

Figure 7. DFT-optimized structures of **4**-1 and **4**-2 (top, perspective view; bottom, side view). The characteristic distances and bond lengths (Å): for **4**-1, B···N(22) 2.995, B−N(23) 1.471, B−N(24) 1.489, B···C(21) 3.158, B···H(21) 2.568, B−C_{ipsoPh} 1.574; for **4**-2, B−N(22) 1.489, B−N(23) 1.473, B···N(24) 3.007, B···C(21) 3.171, B···H(21) 2.570, B−C_{ipsoPh} 1.573.

The optimized geometries of **4**-1 and **4**-2 are shown in Figure 7. They provide evidence for bidentate coordination of N-confused porphyrins. **4**-1 is only slightly more stable, as shown by the DFT studies, because the energy difference between **4**-1 and **4**-2 equals 1.704 kcal/mol. In principle, the small energy difference between **4**-1 and **4**-2 suggests their simultaneous availability. This result seems to be inconsistent with the experimental data, discussed above, which show that the single form, presumably **4**-1, dominates in solution in the whole investigated temperature range.

The DFT-optimized geometries of **5**-syn and **5**-anti are shown in Figure 8. The DFT-determined B−N bond lengths of **5**-OMe closely resemble those determined by the X-ray study for boron porphyrins.[1,2,4,6] However, the addition of

(37) Yamamoto, Y.; Akiba, K. Y. *J. Synth. Org. Chem.* **2004**, *62*, 1128−1137.
(38) Yamashita, M.; Kamura, K.; Yamamoto, Y.; Akiba, K. *Chem.−Eur. J.* **2002**, *8*, 2976−2979.
(39) Yamashita, M.; Yamamoto, Y.; Akiba, K.; Nagase, S. *Angew. Chem., Int. Ed.* **2000**, *39*, 4055−4058.
(40) Yamashita, M.; Yamamoto, Y.; Akiba, K. Y.; Hashizume, D.; Iwasaki, F.; Takagi, N.; Nagase, S. *J. Am. Chem. Soc.* **2005**, *127*, 4354−4371.
(41) Wei, P. R.; Atwood, D. A. *Inorg. Chem.* **1998**, *37*, 4934−4938.
(42) Pawlicki, M.; Latos-Grażyński, L. *Chem.−Eur. J.* **2003**, *9*, 4650−4660.

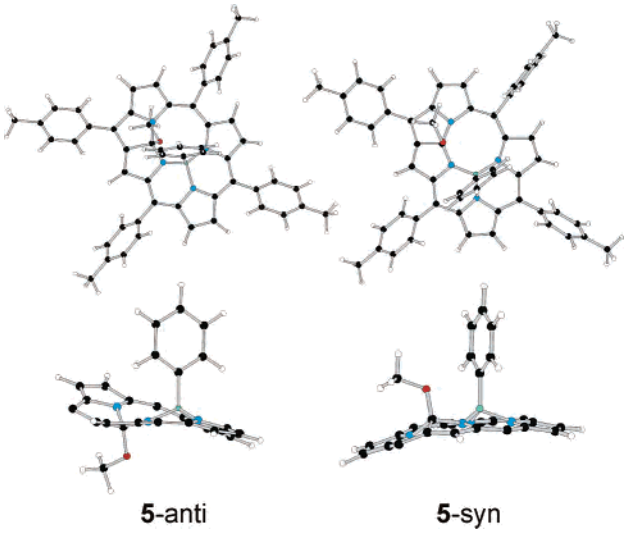

Figure 8. DFT-optimized structure of **5**-anti and **5**-syn (top, perspective view; bottom, side view).

Table 1. Selected DFT-Optimized Bond Lengths and Angles

	3^+	**5**-anti	Δ(**3** − **5**-anti)
C(4)−C(5)	1.414	1.421	−0.007
C(5)−C(6)	1.430	1.415	0.015
C(6)−C(7)	1.395	1.380	0.015
C(7)−C(8)	1.416	1.435	−0.019
C(6)−C(9)	1.440	1.535	−0.095
C(1)−N(21)	1.409	1.382	0.027
C(9)−N(21)	1.360	1.458	−0.098
C(9)−N(22)	1.312	1.420	−0.108
C(8)−N(22)	1.447	1.388	0.059
N(21)−C(9)−C(6)	110.0	100.6	9.4
C(6)−C(9)−N(22)	113.8	104.2	9.6
N(21)−C(9)−N(22)	136.3	119.8	16.5
O−C(9)−C(6)		115.5	
O−C(9)−N(21)		110.5	
O−C(9)−N(22)		106.4	

the methoxide resulted in significant changes in the geometry around the C(9) carbon atom as compared to 3^+ (see Figure 8). Here the marked tendency to acquire the tetrahedral geometry is reflected by the increase of the bond lengths accompanied by the marked decrease of N(21)−C(9)−N(22) and N(22)−C(9)−C(6) angles (Table 1). However, the bond length preserves the conjugated pattern characteristic for the parental molecule 3^+, as shown in Chart 2.

The calculated total electronic energies with zero-point energies, using the B3LYP/6-31G**//B3LYP/6-31G** approach, demonstrate that the anti isomer is more stable, as shown by the DFT studies, because the energy difference equals 5.06 kcal/mol.

A calculation of the hypothetical boron complex, which contains five regular boron−ligand bonds,[36] has been considered as well. The corresponding structural model of **5**-$OMe_{hypervalent}$ involved the use of a fifth coordination site by the methoxy ligand. In spite of the starting point, the optimatization procedure yielded eventually **5**-OMe_{anti}, affording the transfer of methoxide from boron to the C(9) carbon atom.

Conclusions

This study provides insight into the coordinating properties of N-fused porphyrin, which can potentially act as a monoanionic ligand. A preference for the coordination of small metal ions seems to be the inherent property of this contracted porphyrin. It is a consequence of the structural constraints imposed by an N-fused porphyrin structure and the presence of just three nitrogen donors in the molecular cavity. Thus, the present studies add N-fused porphyrin to the class of porphyrinoids that are capable of coordinating to a single boron atom.[11−17] Significantly, 3^+ reveals some features of a boronium cation. This study clearly extends the coordination chemistry with N-fused porphyrins applied as a macrocyclic ligand. The obvious mismatch between the core of an N-confused porphyrin and the boron radius leads to a structure in which the boron is bound by two nitrogen atoms having the σ-phenyl ligand in the third position. In this case, two pyrrole rings including the N-confused ring are not involved in coordination resembling BF_2-coordinated dipyrromethene complexes. The remarkable flexibility of this particular complex structure allows an intermolecular conversion of **4** into 3^+.

Experimental Section

Materials. N-Confused porphyrin (*N*CTTP*H*)H_2 or (*N*CTPP*H*)-H_2 was obtained by methods already described.[43] N-Fused porphyrin was synthesized according to the reported procedure.[20]

From (*N*CTTP*H*)H_2 (1). [3^+]-Cl. 1 (18 mg, 0.027 mmol) was added to 20 mL of toluene under N_2, and $PhBCl_2$ (71 μL, 0.54 mmol, 20 equiv) was then added. The mixture was stirred under reflux and under N_2 for 1 h. The product was chromatographed on the silica gel column. The last fraction (red wine) eluted with CH_2Cl_2/MeOH (10:1) was collected, and solvents were evaporated. After evaporation of the solvents, 4.2 mg was obtained (20%).

From (*N*FTTP)H (2). [3^+]-Cl. 2 (20 mg, 0.030 mmol) was added to 20 mL of toluene under N_2, and $PhBCl_2$ (78 μL, 0.60 mmol, 20 equiv) was then added. The mixture was stirred under reflux and under N_2 for 1 h. The solution was evaporated, and the product was chromatographed on the silica gel column. The last fraction (red wine) eluted with CH_2Cl_2/MeOH (10:1) was collected, and solvents were evaporated. After evaporation of the solvents, 18.5 mg was obtained (78%).

[3^+]-BF_4. $AgBF_4$ in excess was added to the toluene solution of **[3^+]**-Cl. After a few days, the solution was decanted and red oil was dissolved in CH_2Cl_2 and filtered from solid impurities.

The solution was evaporated. The process was almost quantitative.

^{1}H NMR (500 MHz, CD_2Cl_2, 198 K): δ 9.82 (s, 1H, H7), 9.48 (AB, 1H, $^3J_{(H,H)}$ = 5.0 Hz, H3), 8.71 (2H, $^3J_{(H,H)}$ = 8.0 Hz, 5-o), 8.66 (AB, 1H, $^3J_{(H,H)}$ = 4.8 Hz, H2), 8.53 (AB, 1H, $^3J_{(H,H)}$ = 5.0 Hz, H17), 8.45 (1H, $^3J_{(H,H)}$ = 6.9 Hz, 10-o), 8.29 (AB, 1H, $^3J_{(H,H)}$ = 4.6 Hz, H12), 8.18 (AB, 1H, $^3J_{(H,H)}$ = 4.6 Hz, H13), 8.15 (1H, $^3J_{(H,H)}$ = 7.8 Hz, 20-o), 8.11 (1H, $^3J_{(H,H)}$ = 7.9 Hz, 20-o), 8.06 (AB, 1H, $^3J_{(H,H)}$ = 5.0 Hz, H18), 8.06 (1H $^3J_{(H,H)}$ = 7.8 Hz, 10-o), 7.79 (1H, $^3J_{(H,H)}$ = 7.3 Hz, 10-m), 7.72 (1H, $^3J_{(H,H)}$ = 7.8 Hz, 10-m), 7.68 (1H, $^3J_{(H,H)}$ = 8.3 Hz, 15-o), 7.63 (4H, $^3J_{(H,H)}$ = 7.6 Hz, 5-m, 20-m), 7.53 (1H, $^3J_{(H,H)}$ = 7.6 Hz, 15-m), 7.29 (1H, $^3J_{(H,H)}$ = 7.8 Hz, 15-m), 6.92 (1H, $^3J_{(H,H)}$ = 7.3 Hz, 15-o), 6.28 (tr, 1H, $^3J_{(H,H)}$ = 7.2 Hz, *p*-Ph), 5.99 (tr, 2H, $^3J_{(H,H)}$ = 7.8 Hz, *m*-Ph), 3.48 (d, 2H, $^3J_{(H,H)}$ = 7.8 Hz, *o*-Ph), 2.67 (s, 3H, 10-Me), 2.57 (s, 3H, 15-Me), 2.56 (s, 3H, 5- or 20-Me), 2.53 (s, 3H, 20- or 5-Me). ^{13}C NMR

(43) Geier, G. R., III; Haynes, D. M.; Lindsey, J. S. *Org. Lett.* **1999**, *1*, 1455−1458.

(125.7 MHz, $CDCl_3$, 298 K): δ 151.7, 147.9, 145.6, 143.8, 142.2, 142.0, 141.7, 141.2, 140.8, 140.7, 139.7, 139.4, 138.3, 137.4, 136.9, 133.1, 133.0, 132.1, 131.8, 131.3, 131.3, 130.6, 130.5, 130.2, 130.0, 130.0, 129.8, 128.9, 127.8, 127.8, 127.4, 127.2, 125.9, 119.4, 116.5, 114.3, 21.8, 21.7, 21.5. ^{11}B NMR (160.5 MHz, $CDCl_3$, 298 K): δ −1.4 (BF_4^-), −6.8. UV−vis: λ_{max}, nm (log ϵ) 337 (4.44), 386 (4.43), 499 (4.85), 569 (4.33), 756 (4.43), 926 (3.58), 1051 (5.59). HRMS (ESI, *m*/*z*): 754.3452 [calcd 754.3382 for $[C_{54}H_{40}N_4B]^+$ (M^+)].

4. 1 (18 mg, 0.027 mmol) was added to 20 mL of toluene under N_2. Subsequently, $PhBCl_2$ (71 μL, 0.54 mmol, 20 equiv) was added. The mixture was stirred under reflux and under N_2 for 1 h. The product was chromatographed on the silica gel column with toluene as the eluent. The first fraction (toluene) was collected, and the solvent was evaporated. Yield: 12.2 mg, 60%.

^{1}H NMR (500 MHz, toluene-d_8, 298 K): δ 10.04 (d, 1H, $^4J_{(H,H)}$ = 0.9 Hz, H3), 8.92 (AB, 1H, $^3J_{(H,H)}$ = 4.8 Hz, H12), 8.80 (AB, 1H, $^3J_{(H,H)}$ = 4.8 Hz, H13), 8.54 (AB, 1H, $^3J_{(H,H)}$ = 4.7 Hz, H8), 8.48 (AB, 1H, $^3J_{(H,H)}$ = 4.6 Hz, H18), 8.39 (AB, 1H, $^3J_{(H,H)}$ = 4.7 Hz, H17), 8.38 (2H, $^3J_{(H,H)}$ = 8.1 Hz, 5-o), 8.32 (AB, 1H, $^3J_{(H,H)}$ = 4.8 Hz, H7), 8.22 (v br, 2H, 20-o), 8.02 (1H, $^3J_{(H,H)}$ = 6.8 Hz, 10-o), 7.91 (1H, $^3J_{(H,H)}$ = 6.8 Hz, 10-o), 7.86 (2H, $^3J_{(H,H)}$ = 7.8 Hz, 15-o), 7.40 (1H, $^3J_{(H,H)}$ = 6.4 Hz, 20-m), 7.28 (2H, $^3J_{(H,H)}$ = 7.8 Hz, 5-m), 7.25 (s, br, 1H, 20-m), 7.22 (2H, $^3J_{(H,H)}$ = 7.9 Hz, 15-m), 5.99 (tr, 1H, $^3J_{(H,H)}$ = 7.3 Hz, *p*-Ph), 5.87 (tr, 2H, $^3J_{(H,H)}$ = 7.6 Hz, *m*-Ph), 3.36 (d, 2H, $^3J_{(H,H)}$ = 7.1 Hz, *o*-Ph), 2.48 (s, 3H, 10-Me), 2.44 (s, 3H, 20-Me), 2.33 (s, 3H, 5-Me), 2.31 (s, 3H, 15-Me), −2.23 (s, 1H, H21). ^{1}H NMR (500 MHz, toluene-d_8, 213 K): δ 10.21 (s, 1H, H3), 9.08 (AB, 1H, $^3J_{(H,H)}$ = 4.6 Hz, H12), 9.01 (AB, 1H, $^3J_{(H,H)}$ = 4.6 Hz, H13), 8.71 (1H, $^3J_{(H,H)}$ = 7.6 Hz, 20-o), 8.61 (AB, 1H, $^3J_{(H,H)}$ = 4.6 Hz, H8), 8.52 (AB, 1H, $^3J_{(H,H)}$ = 4.4 Hz, H18), 8.38 (AB, 1H, $^3J_{(H,H)}$ = 4.4 Hz, H17), 8.35 (2H, $^3J_{(H,H)}$ = 7.6 Hz, 5-o), 8.27 (AB, 1H, $^3J_{(H,H)}$ = 4.2 Hz, H7), 8.04 (1H, $^3J_{(H,H)}$ = 7.3 Hz, 10-o), 7.95 (1H, $^3J_{(H,H)}$ = 8.0 Hz, 10-o), 7.84 (1H, $^3J_{(H,H)}$ = 7.8 Hz, 15-o), 7.80 (1H, $^3J_{(H,H)}$ = 7.6 Hz, 15-o), 7.69 (1H, $^3J_{(H,H)}$ = 7.6 Hz, 20-o), 7.50 (1H, $^3J_{(H,H)}$ = 7.3 Hz, 20-m), 7.30 (3H, $^3J_{(H,H)}$ = 7.1, 2 × 5-m, 10-m), 7.23 (1H, $^3J_{(H,H)}$ = 7.1 Hz, 20-m), 7.18 (3H, 2 × 15-m, 10-m), 6.07 (tr, 1H, $^3J_{(H,H)}$ = 7.0 Hz, *p*-Ph), 5.96 (tr, 2H, $^3J_{(H,H)}$ = 7.6 Hz, *m*-Ph), 3.44 (d, 2H, $^3J_{(H,H)}$ = 7.3 Hz, *o*-Ph), 2.46 (s, 3H, 10-Me), 2.43 (s, 3H, 20-Me), 2.34 (s, 3H, 5-Me), 2.32 (s, 3H, 15-Me), −2.35 (s, 1H, 21H). ^{13}C NMR (125.7 MHz, CD_2Cl_2, 298 K): δ 154.2, 153.8, 151.4, 144.5, 144.2, 143.9, 140.1, 138.7, 137.7, 137.3, 137.2, 137.1, 136.1, 135.6, 135.4, 134.2, 134.1, 133.8, 132.6, 132.3, 131.3, 130.4, 129.8, 129.1, 128.6, 128.2, 127.1, 126.5, 125.3, 124.4, 123.3, 121.9, 119.5, 116.1, 115.5, 115.0, 111.3, 110.3, 72.5, 31.9, 29.7, 29.3, 22.7, 21.2, 21.1, 21.1, 13.9. ^{11}B NMR (160.5 MHz, $CDCl_3$, 298 K): δ −11.8. UV−vis: λ_{max}, nm (log ϵ): 366 (4.30), 421 (4.29), 493 (4.68), 657 (3.91), 725 (3.77). HRMS (ESI, *m*/*z*): 754.3365 [calcd 754.3382 for $[C_{54}H_{40}N_4B]^+$ ($[M - H]^+$ as **4** converts into $\mathbf{3}^+$ during the ESI experiment)].

5-OMe. $\mathbf{3}^+$ (3.1 mg) was dissolved in dichloromethane, and MeONa in methanol was added. The progress of the reaction was controlled by UV−vis. Once the reaction was completed, the solvents were evaporated. The product was dissolved in CH_2Cl_2, and solid impurities were filtered off. Yield: 1.5 mg, 52%.

^{1}H NMR (500 MHz, CD_2Cl_2, 203 K): δ 10.14 (s, 1H, H7), 8.79 (AB, 1H, $^3J_{(H,H)}$ = 4.6 Hz, H18), 8.65 (AB, 1H, $^3J_{(H,H)}$ = 4.6 Hz, H12), 8.61 (2H, $^3J_{(H,H)}$ = 7.1 Hz, 5-o), 8.60 (AB, 1H, $^3J_{(H,H)}$ = 3.4 Hz, H2), 8.56 (AB, 1H, $^3J_{(H,H)}$ = 4.4 Hz, H3), 8.52 (1H, $^3J_{(H,H)}$ = 7.6 Hz, 10-o), 8.41 (AB, 1H, $^3J_{(H,H)}$ = 4.6 Hz, H17), 8.26 (1H, $^3J_{(H,H)}$ = 8.5 Hz, 20-o), 8.19 (AB, 1H, $^3J_{(H,H)}$ = 4.6 Hz, H13), 8.16 (1H, $^3J_{(H,H)}$ = 7.6 Hz, 15-o (anti to σ-phenyl, NOE correlated to −OMe)), 7.82 (1H, $^3J_{(H,H)}$ = 7.6 Hz, 20-o), 7.75 (2H, $^3J_{(H,H)}$ = 7.3 Hz, 10-m), 7.63 (1H, $^3J_{(H,H)}$ = 7.3 Hz, 20-m), 7.58 (2H, $^3J_{(H,H)}$ = 7.6 Hz, 5-m), 7.54 (2H, $^3J_{(H,H)}$ = 8.7 Hz, 15-m, 20-m), 7.51 (1H, $^3J_{(H,H)}$ = 8.0 Hz, 10-o), 7.30 (1H, $^3J_{(H,H)}$ = 6.6 Hz, 15-m), 7.17 (1H, $^3J_{(H,H)}$ = 7.8 Hz, 15-o (syn to σ-phenyl, NOE correlated to σ-phenyl)), 5.65 (tr, 1H, $^3J_{(H,H)}$ = 7.2 Hz, *p*-Ph), 5.26 (tr, 2H, $^3J_{(H,H)}$ = 7.8 Hz, *m*-Ph), 2.61 (s, 3H, 20-Me), 2.59 (s, 6H, 10- and 15-Me), 2.51 (s, 3H, 5-Me), 1.80 (d, 2H, $^3J_{(H,H)}$ = 7.6 Hz, *o*-Ph), −0.54 (s, 3H, −OMe). ^{13}C NMR (125.7 MHz, CD_2Cl_2, 298 K): δ 154.4, 150.6, 147.7, 143.6, 143.5, 141.8, 141.7, 138.3, 137.9, 137.8, 137.5, 137.2, 135.7, 135.6, 134.9, 134.5, 134.4, 134.1, 133.5, 133.3, 132.8, 131.7, 130.9, 130.1, 129.5, 129.2, 127.6, 127.6, 127.0, 126.8, 125.3, 124.8, 124.3, 123.0, 119.4, 115.9, 115.1, 113.8, 112.5, 95.2 (C9), 46.4, 21.6, 21.5, 21.5. ^{11}B NMR (160.5 MHz, $CDCl_3$, 298 K): δ −12.9. UV−vis: λ_{max}, nm (log ϵ): 331 (4.39), 401 (4.44), 425 (4.48), 503 (4.82), 538 (4.58), 680 (4.16). HRMS (ESI, *m*/*z*): 754.3322 [calcd 754.3382 for $[C_{54}H_{40}N_4B]^+$ ($[M - OMe]^+$)].

5-OR. The synthesis of other alkoxide adducts followed the procedure described for **5**-OMe.

5-OEt. ^{1}H NMR (500 MHz, $CDCl_3$, 298 K), the alkoxy fragment: δ −0.52 (m, 1H, −OCH*H*−), −0.68 (m, 1H, −OC*H*H−), −1.04 (tr, 3H, $-CH_3$).

5-OBu. ^{1}H NMR (500 MHz, $CDCl_3$, 298 K), the alkoxy fragment: δ −0.42, −0.61, −0.74, −0.85, −0.91, −0.99.

5-O(CH$_2$)$_2$OH. ^{1}H NMR (500 MHz, $CDCl_3$, 298 K), the alkoxy fragment: δ 1.50, −0.01, −0.74, −1.00.

DFT Calculations. DFT calculations for structures **4** and **5**-OMe were performed with the *GAUSSIAN03* program.[44] Geometry optimizations were carried out within unconstrained C_1 symmetry, with the starting coordinates derived from X-ray structural data. Becke's three-parameter exchange functionals[45] with the gradient-corrected correlation formula of Lee, Yang, and Parr [DFT-(B3LYP)][46] were used with the 6-31G** basis set.[47] Harmonic vibrational frequencies were calculated using analytical second derivatives. Structures were found to have converged to a minimum on the potential energy surface.

Instrumentation. NMR spectra were recorded on a Bruker Avance 500 spectrometer. UV−vis electronic spectra were recorded on a diode-array Hewlett-Packard 8453 spectrometer and Varian Cary 50 Bio. Mass spectra were recorded on a Bruker micrOTOF-Q spectrometer using the electrospray and liquid-matrix secondary-ion mass spectrometry techniques.

EPR spectra were obtained with a Bruker ESP 300E spectrometer. The magnetic field was calibrated with a proton magnetometer and EPR standards.

(44) Frisch, M. J.; Trucks, G. W.; Schlegel, H. B.; Scuseria, G. E.; Robb, M. A.; Cheeseman, J. R.; Montgomery, J. A., Jr.; Vreven, T.; Kudin, K. N.; Burant, J. C.; Millam, J. M.; Iyengar, S. S.; Tomasi, J.; Barone, V.; Mennucci, B.; Cossi, M.; Scalmani, G.; Rega, N.; Petersson, G. A.; Nakatsuji, H.; Hada, M.; Ehara, M.; Toyota, K.; Fukuda, R.; Hasegawa, J.; Ishida, M.; Nakajima, T.; Honda, Y.; Kitao, O.; Nakai, H.; Klene, M.; Li, X.; Knox, J. E.; Hratchian, H. P.; Cross, J. B.; Adamo, C.; Jaramillo, J.; Gomperts, R.; Stratmann, R. E.; Yazyev, O.; Austin, A. J.; Cammi, R.; Pomelli, C.; Ochterski, J. W.; Ayala, P. Y.; Morokuma, K.; Voth, G. A.; Salvador, P.; Dannenberg, J. J.; Zakrzewski, V. G.; Dapprich, S.; Daniels, A. D.; Strain, M. C.; Farkas, O.; Malick, D. K.; Rabuck, A. D.; Raghavachari, K.; Foresman, J. B.; Ortiz, J. V.; Cui, Q.; Baboul, A. G.; Clifford, S.; Cioslowski, J.; Stefanov, B. B.; Liu, G.; Liashenko, A.; Piskorz, P.; Komaromi, I.; Martin, R. L.; Fox, D. J.; Keith, T.; Al-Laham, M. A.; Peng, C. Y.; Nanayakkara, A.; Challacombe, M.; Gill, P. M. W.; Johnson, B.; Chen, W.; Wong, M. W.; Gonzalez, C.; Pople, J. A. *Gaussian 03*, revision C.01; Gaussian: Pittsburgh, PA, 2004.
(45) Becke, A. D. *Phys. Rev. A* **1988**, *38*, 3098−3100.
(46) Lee, C.; Yang, W.; Parr, R. G. *Phys. Rev. B* **1988**, *37*, 785−789.
(47) Hay, P. J.; Wadt, W. R. *J. Chem. Phys.* **1985**, *82*, 270−283, 284−298, and 299−310.

X-ray Analysis. X-ray-quality crystals of $\mathbf{3}^+$ were prepared by diffusion of decane into a dichloromethane solution contained in a thin tube. Data were collected at 100 K on an Xcalibur PX κ-geometry diffractometer with a CCD Onyx camera. The data were corrected for Lorentz and polarization effects. Numerical absorption correction was applied. Crystal data are compiled in Table S1 in the Supporting Information. The structure was solved by direct methods with *SHELXS-97* and refined by the full-matrix least-squares method by using *SHELXL-97* with anisotropic thermal parameters for the non-hydrogen atoms. Scattering factors were those incorporated in *SHELXS-97*.[48,49]

The asymmetric unit contains one $\mathbf{3}^+$ cation and a chloride anion accompanied by 2.52 molecules of dichloromethane distributed over four independent sites. The chloride anion was refined as disordered over two crystallographically independent sites and assumed to accidentally overlap with chlorine atoms of a CH_2Cl_2 molecule disordered around an inversion center (0.22 occupancy).

(48) Sheldrick, G. M. *SHELXS97, program for solution of crystal structures*; University of Göttingen: Göttingen, Germany, 1997.
(49) Sheldrick, G. M. *SHELXL97, program for crystal structure refinement*; University of Göttingen: Göttingen, Germany, 1997.

Electrochemistry. Electrochemical measurements were performed in CH_2Cl_2 with tetrabutylammonium perchlorate as the supporting electrolyte. Cyclic voltammograms were recorded for the potential scan rate ranging from 0.05 to 0.2 V/s using the EA9C (MIM, Kraków, Poland) apparatus. A glassy-carbon working electrode, a Pt-wire auxiliary electrode, and an Ag/AgCl reference electrode were applied.

Acknowledgment. Financial support from the Ministry of Science and Higher Education (Grant PBZ-KBN-118/T09/2004) is kindly acknowledged. Quantum chemical calculations have been carried out at the Poznań Supercomputer Center (Poznań, Poland) and Wrocław Supercomputer Center (Wrocław, Poland).

Supporting Information Available: X-ray crystallographic data in CIF format, tables of computational results (Cartesian coordinates), and additional NMR data. This material is available free of charge via the Internet at http://pubs.acs.org.

IC700647V